NANO LETTERS

Letter

pubs.acs.org/NanoLett

Direct Observation of a Long-Lived Single-Atom Catalyst Chiseling Atomic Structures in Graphene

Wei Li Wang,[†,‡] Elton J. G. Santos,[‡] Bin Jiang,[§] Ekin Dogus Cubuk,[‡] Colin Ophus,[∥] Alba Centeno,[⊥] Amaia Pesquera,[⊥] Amaia Zurutuza,[⊥] Jim Ciston,[∥] Robert Westervelt,[†,‡] and Efthimios Kaxiras*[,†,‡]

[†]Department of Physics, Harvard University, Cambridge, Massachusetts 02138, United States

[‡]School of Engineering and Applied Sciences, Harvard University, Cambridge, Massachusetts 02138, United States

[§]FEI Corporation, 5350 NE Dawson Creek Drive, Hillsboro, Oregon 97124, United States

[∥]National Center for Electron Microscopy, Lawrence Berkeley National Laboratory, Berkeley, California 94720, United States

[⊥]Graphenea S.A., 76 Tolosa Hiribidea, Donostia-San Sebastian, E-20018, Spain

Supporting Information

ABSTRACT: Fabricating stable functional devices at the atomic scale is an ultimate goal of nanotechnology. In biological processes, such high-precision operations are accomplished by enzymes. A counterpart molecular catalyst that binds to a solid-state substrate would be highly desirable. Here, we report the direct observation of single Si adatoms catalyzing the dissociation of carbon atoms from graphene in an aberration-corrected high-resolution transmission electron microscope (HRTEM). The single Si atom provides a catalytic wedge for energetic electrons to chisel off the graphene lattice, atom by atom, while the Si atom itself is not consumed. The products of the chiseling process are atomic-scale features including graphene pores and clean edges. Our experimental observations and first-principles calculations demonstrated the dynamics, stability, and selectivity of such a single-atom chisel, which opens up the possibility of fabricating certain stable molecular devices by precise modification of materials at the atomic scale.

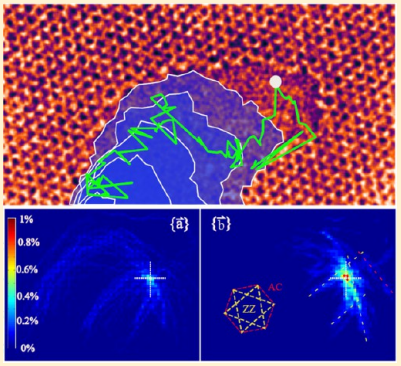

KEYWORDS: *Single-atom catalyst, graphene, HRTEM, molecular devices*

Known to humans for centuries, catalysts play an enabling role in many chemical processes that are crucial to modern society. Recent advances in nanotechnology introduced nanocatalysts[1] that enable the creation of novel nanostructures such as carbon nanotubes[2,3] and semiconductor nanowires.[4] The characteristics of the resulting stable nanostructures can be tuned by the structures of the corresponding nanocatalysts. For example, in the growth of semiconductor nanowires from metal nanoparticles in a vapor−liquid−solid process,[4] the diameter of the resultant nanowire is determined by the size of the catalytic nanoparticles. It is not clear what is the smallest catalyst particle that can be used to control the features of the resultant nanostructures and what is the catalytic mechanism involved in such a limiting scenario. A catalytic process typically involves complex atomic-scale bond breaking and reforming events that are hard to resolve either spatially or temporally. High-resolution imaging techniques employing STM probes[5] and scanning electron probes[6,7] have been used to image single-atom catalysts embedded in a host surface, but the slow frame rate of these probes makes it difficult to obtain a continuous picture of the catalytic process. In this work, using aberration-corrected high-resolution transmission electron microscopy (HRTEM), we directly observed the dynamic process in which a single Si atom acts as a catalyst and produces atomic structures in graphene under electron irradiation. This single-atom catalyst has a very long lifetime even though it is not supported by any host surface other than the graphene structure that it binds to and helps to sculpt.

An unprecedented 2D material, graphene presents unique opportunities for fabricating functional molecular devices with a top-down approach. Many novel electronic and spintronic properties of graphene nanostructures and graphene edges have been proposed and studied.[8−10] Various approaches have been tried to sculpt graphene devices employing electron beams,[11,12] energetic ions,[13,14] nanoparticles,[15,16] or scanning probes.[17] However, achieving atomically well-defined graphene features remains a challenge because it is difficult to obtain an effective atomic-sized fabrication tool. The single catalyst atom shown here is the smallest possible fabrication tool, which can significantly modify the local energy landscape, and selectively produce high-quality functional atomic-sized features under electron irradiation.

We use the TEAM 0.5 transmission electron microscope (TEM) at the National Center of Electron Microcopy (NCEM) for imaging and in situ fabrication. Our monolayer graphene samples were produced from a standard chemical

Received: September 5, 2013
Revised: January 20, 2014
Published: January 21, 2014

dx.doi.org/10.1021/nl403327u | *Nano Lett.* 2014, 14, 450−455

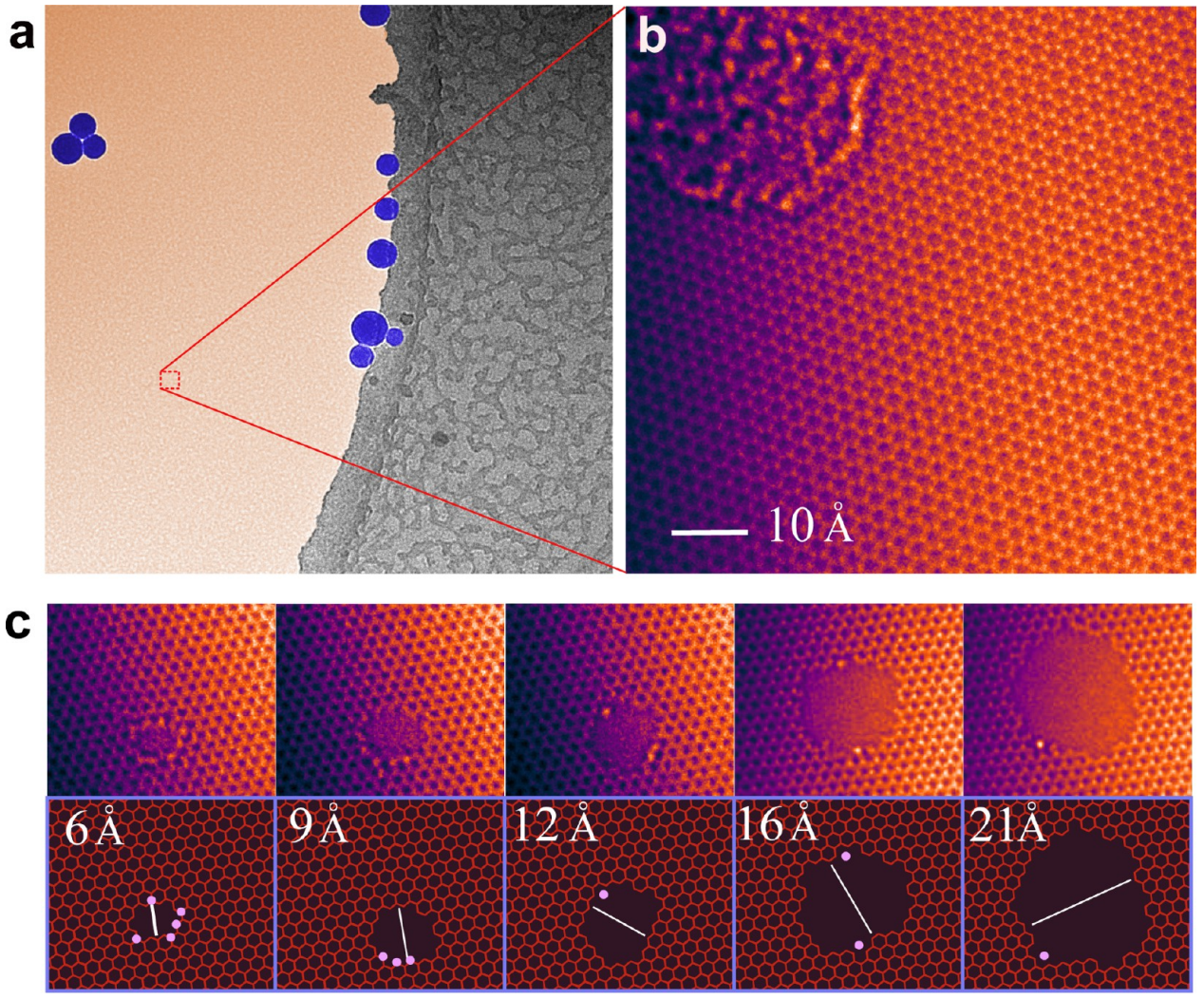

Figure 1. Unfiltered TEM images of a suspended single layer graphene sample with silicon adatoms and the pore-opening process. (a) The edge of one TEM grid hole covered by a single-layer graphene sample (highlighted with light orange color). The sample is decorated with SiO_2 nanoparticles (highlighted with deep blue color), mostly clustered on either suspended graphene or the carbon grid. (b) High-resolution image of the suspended graphene sample showing coexistence of clean pristine graphene and aggregation of impurities (upper left corner). (c) Images of molecular-scale graphene pores of various sizes, with mobile catalyst Si atoms on the edges. The lower panel images illustrate the corresponding atomic configurations.

vapor deposition (CVD) process and transferred subsequently to standard holey carbon TEM grids. Silicon dioxide impurities are introduced unintentionally into the samples during the transferring process. Besides the clustered SiO_2 nanoparticles shown in Figure 1a, another form of impurity includes patches of thin adsorbed hydrocarbon layer, shown in the upper left corner of Figure 1b. We performed electron energy loss spectroscopy (EELS) in situ in the TEM on both types of the impurities and found a clear signature of Si and O elements (see Supporting Information), but no trace of previously studied[18−20] transition metal species such as Co, Ni, Cu, and so forth. The impurity patches can be easily cleaned away with electron beam irradiation (80 kV) and leave a clean pristine single layer graphene areas, as shown in Figure 1b.

Clean graphene is robust against electron irradiation at 80 kV,[21] but occasionally we observed the formation of single Si substitutional defects, as shown in Figure 2a. The Si atoms in such configurations arrive at the defect sites by surface diffusion, in the form of single Si adatoms that have a high mobility on graphene due to a small diffusion barrier.[22] The fast diffusing Si adatom cannot be resolved at each step of its motion, but once it becomes a substitutional defect it is stable enough to be imaged.[18] In addition to such single atom substitutional defects, we also observed the initiation of pore opening. (See Movie S1 in the Supporting Information.) The width of the pore starts from only a few angstroms and gradually increases with the presence of Si adatoms and under continuous electron irradiation. This Si-assisted pore opening process is highly selective and stable; that is, the dissociation and loss of C atoms are highly correlated with the position of the Si atoms which are not being consumed (removed) during the processes. If the concentration of Si atoms is carefully controlled, the electron irradiation can be limited to an area where there is a single defect, initiating the opening of a single pore in graphene. The pore size can be controlled by stopping the irradiation at any moment when the desired size has been reached, as shown in Figure 1c. These molecular-sized pores are excellent candidates for molecular detection applications, such as rapid DNA sequencing,[11,23] because they can be tuned to

dx.doi.org/10.1021/nl403327u | *Nano Lett.* 2014, 14, 450−455

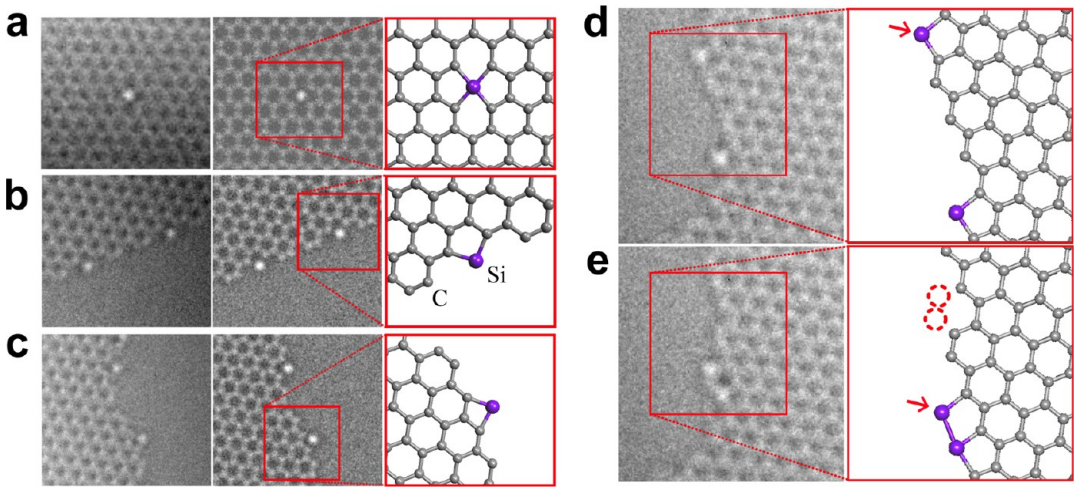

Figure 2. Observed and simulated static and dynamic configurations of single Si adatoms in graphene. a, b, and c are static configurations corresponding to single Si substitutional defects, Si atoms adsorbed to the armchair edge, and to the zigzag edge, respectively. For each configuration, we show the raw TEM images (left), the TEM simulations (center), and the atomic models (right). (d and e) Consecutive TEM images (left) acquired 2.6 s apart showing the movement of one (pointed by red arrow) of the two Si adatoms and the removal of the two neighboring C atoms (positions circled with red dashed lines).

match the size of a single DNA molecule (~10 Å) for the sensitivity that is needed for single base recognition.

Figure 2a shows a single substitutional defect, which is important in initializing the process of pore opening, as shown in Movie S1. Once the pore is open, it is energetically favorable for the Si adatoms to be trapped in the pore. At the edge of the pores, the Si adatoms are mainly observed at the armchair edge as shown in Figure 2b, although rarely they are also found at the zigzag edge as shown in Figure 2c. Figure 2d and e captures the removal of a pair of C atoms catalyzed by the presence of a Si adatom nearby: These two images are 2.6 s apart and clearly show that the pair of edge C atoms nearest to one of the two Si atoms have been removed while this Si atom moved to a position next to another Si atom also at the edge of the pore. This indicates that the Si adatom weakens the binding of neighboring C atoms and makes it easy to remove them from graphene with the help of incident electrons.

To confirm the observed C atom removal mechanism and reveal the details of the process, we performed first-principles calculations on both the static binding energy and the energy paths of dynamic bond disassociation events. It has been shown that various metal atoms, once adsorbed on the graphene surface, lower the defect formation energies.[24] We calculated the change of binding energy for a C atom in graphene when a Si adatom is chemisorbed on top of it and found a reduction of 1.9 eV in the binding energy (16 eV without Si). This reduction is substantial considering that the 80 kV imaging electrons provide an excitation energy that is close to the removal threshold.[12] A close examination of the charge difference density plot (Figure 3a) shows that all of the neighboring C−C bonds of the C atom to which Si is bonded are weakened due to the bonding between this C atom and the Si adatom or due to the direct interaction between the Si and the neighboring C atoms. This renders the Si-bonded C atom vulnerable to removal by incoming electrons. We also calculated multiple-Si configurations (Table 1) and found a further significant binding energy reduction. This is consistent with our observations that pores usually open faster in the presence of multiple Si atoms. The Si atoms at the pore edges bond to the edge C atoms covalently, as indicated in Figure 3b by the charge accumulation between the Si and its nearest neighbor C. In contrast, there is a significant charge depletion in the bonds connecting the nearest C atoms to the second nearest neighbor C atoms along the edge. As a result, the binding energy of the latter is reduced by 1.1 eV.

The binding energy gives a direct description of the bond weakening mechanism. To calculate the removal (displacement) cross section of C atoms, it is important to find the threshold scattering-electron energy that is needed to overcome the energy barrier for removing a C atom. We performed MD simulations for various configurations considered above to obtain the threshold energies, which are then used in the calculation of scattering cross sections, as shown in Figure 3c. It is clear that pristine graphene (with threshold for C atom removal of 21.9 eV) has a vanishing cross section for C atom removal at 80 kV. The adsorption of Si substantially increases the cross section to 0.51 barn or 4.21 barn with the two-Si configuration SiG-Si. These differences indicate that Si can act as a catalyst with excellent selectivity and makes it possible to open graphene pores and leave the surrounding pristine graphene intact when both areas are subject to the same electron irradiation. For the edge configuration, the absorption of Si atom accounts for an increase of the C atom removal cross section by more than 20 times, indicating that the continuous sculpting of graphene features is dominated by the catalytic effect of single Si adatoms.

In Figure 4 (Movie S2 in the Supporting Information), we show a single Si atom caught in action catalyzing the bond dissociation in a graphene pore. The instantaneous positions of the single Si atom obtained from the 100 snapshots are connected by straight lines to form a pseudo trajectory (limited by temporal resolution). The pore area increases linearly as a function of time as shown in Figure 4b. This is a clear indication that the C atom removal events are dominated by the single Si catalyst atom instead of by the loss of C atoms along the edge, because otherwise the increase of the pore area would be superlinear in time as the edge length increases.

In Figure 4c, we compare two vector distributions to show the spatial correlation between the single Si atom and the removal of graphene lattice sites. Two vectors are defined as $\vec{a}$ =

dx.doi.org/10.1021/nl403327u | Nano Lett. 2014, 14, 450−455

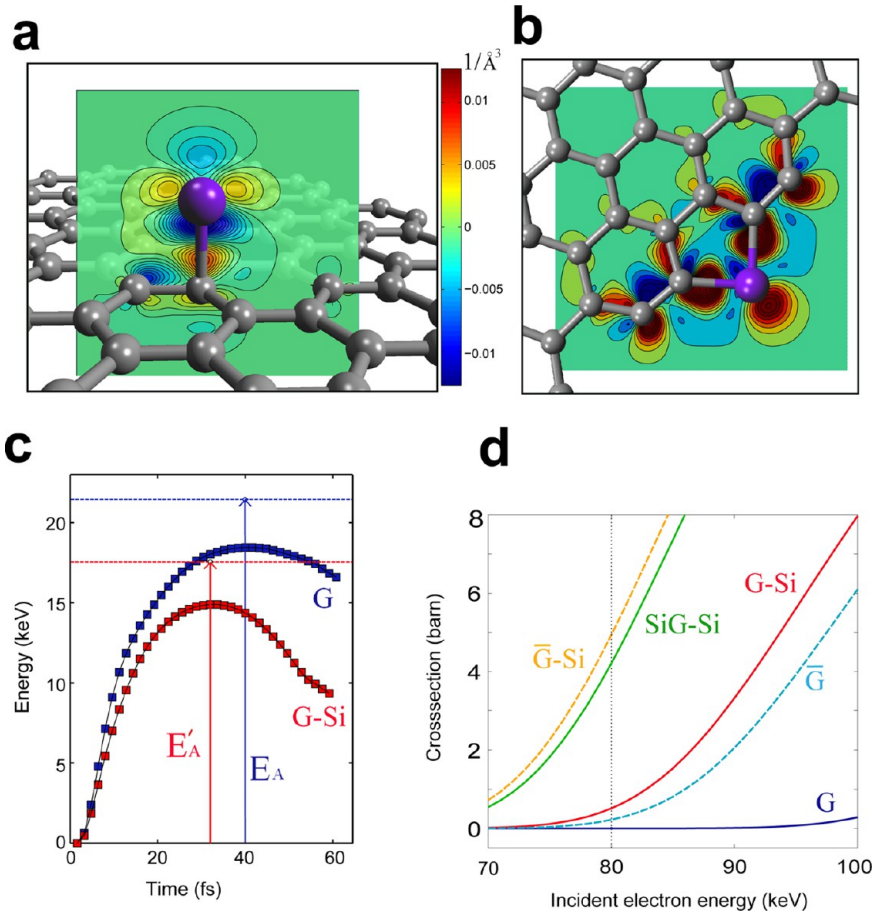

Figure 3. Proposed catalytic mechanism of the single Si adatom on graphene and its edges. (a) Charge density difference contour plot of a single Si atom adsorbed on graphene. (The charge density of the graphene system without the Si adatom and that of the isolated Si atom were subtracted from that of the graphene system with the Si adatom.) The plot plane slices through one of the bonds of the C atom that is bonded to a Si adatom, showing a significantly reduced charge density in the bonding area. The positive and negative region in the Si−C bond shows the ionic nature of the bond. (b) Charge density difference contour plot of a single Si atom adsorbed to the arm-chair edge of graphene. The Si atom (highlighted with purple color) is bonded to its nearest C atoms with covalent bonds which in turn weakens the neighboring bonds along the edge that connect to the second nearest neighbor C atoms, as is indicated by the substantial reduction of charge density in the neighboring bond regions. (c) Energy profiles from a first-principles MD simulation of an event where a single C atom is removed from the graphene system due to the collision with incident electrons. The plotted curves are the time history of the total system potential energy during the event. By adding the kinetic energy transferred to the rest of the system, the dashed lines above the curves show the threshold energy that is required to make the removal event possible. We show two curves and threshold energies E'_A and E_A for a C atom in graphene with and without a bonded Si adatom. The former shows a reduction of the threshold energy by 4.5 eV. (d) The calculated C atom removal cross sections for various graphene-Si adatom configurations, which in increasing order are: pristine graphene (G), graphene armchair edge ($\overline{G}$), graphene with Si adatom (G-Si), graphene with single substitute defect and a Si adatom (SiG-Si), and graphene armchair edge with single Si adatom ($\overline{G}$-Si).

$\vec{r}_e - \vec{r}_{Si}$ and $\vec{b} = \vec{r}'_p - \vec{r}_{Si}$, where $\vec{r}_{Si}$ is the instantaneous position of the single Si atom in a snapshot, $\vec{r}_e$ is the position of an edge pixel (identified as graphene edge through image processing), and $\vec{r}'_p$ is the position of a "just removed" edge pixel which is identified by comparing two adjacent snapshots. There is a vector $\vec{a}$ associated with each edge pixel in all snapshots, while there is a vector $\vec{b}$ associated with a pixel only if this edge pixel is removed in the next snapshot. The two spatial distribution plots are based on the vector sets $\{\vec{a}\}$ and $\{\vec{b}\}$ that include all identified vectors from the 100 snapshots through image processing. Compared to the distribution of $\{\vec{a}\}$ (left panel), the distribution of $\{\vec{b}\}$ (right panel) is peaked around the origin. This shows that the C atoms removed by electrons are highly correlated spatially with the hopping single Si atom, which again confirms the activity of the single-atom Si catalyst. The distribution of $\{\vec{b}\}$ has certain directionality along the zigzag and armchair orientations of the lattice, with a preference on the zigzag direction. The observation in Figure 4 demonstrates the remarkable stability of the single atomic catalyst which significantly and locally increases the removal rate of C atoms while the catalyst Si atom is not consumed by the process.

It is not entirely clear if Si is a unique element in terms of catalyzing the bond dissociation in graphene. Recent scanning TEM studies[18−20] showed evidence that transition metal atoms are present at the edges and may help the "etching" of graphene. However, it was reported that these atoms are consumed, and then the "etching" stops. Our observation and analysis indicate that Si may represent an optimal choice between lower and higher atomic number elements for catalytic behavior in graphene: Lighter atoms can bond to graphene strongly as Si does, but they suffer from a larger momentum transfer from electrons during scattering and are prone to be sputtered away. Heavier elements gain less momentum from

dx.doi.org/10.1021/nl403327u | Nano Lett. 2014, 14, 450−455

Table 1. Binding Energies, Dynamic Threshold Energies for C Atom Removal, and the Corresponding Cross Section for Various Graphene Features with and without the Single Si Catalyst Adatom[a]

item	G	G-Si	SiG-Si	$\overline{G}$	$\overline{G}$-Si
E_b (eV)	16.0	14.1	11.8	11.2	10.1
E_A (eV)	21.9	17.4	15.4	18.0	15.2
σ_{80} (barn)	9.52×10^{-5}	0.51	4.21	0.22	4.93

[a]The binding energy of a C atom is defined as $E_b = E_v + E_s - E_T$ where E_v is the total energy of a feature with the C atom position vacant, E_s is the total energy of the C atom, and E_T is the total energy of the feature. The activation energy E_A is obtained from the MD simulations discussed in the text. The C atom removal cross section σ_{80} is the cross section measured in units of barn for the given incident electron energy of 80 kV. The configurations are defined as follows. G: graphene; $\overline{G}$: graphene edge in the armchair configuration; G-Si: graphene with a Si adatom (as shown in Figure 3a); $\overline{G}$-Si: graphene edge with a Si adatom (as shown in Figure 2b); SiG-Si: a single Si substitutional defect (as shown in Figure 2a) and an additional Si adatom on one of the neighboring C atoms.

colliding electrons, but they typically bond to graphene less strongly and thus are consumed in the process. The Si−C bond is strong enough to ensure that Si keeps holding on to the edge of graphene, and the Si atom is heavy enough to avoid excessive momentum transfer from electrons.

The chiseling mechanism of the long-lived single-atom catalyst we demonstrated here should not be unique for Si binding to graphene. There are likely other atomic chisel−substrate pairs existing in nature. We also expect the chiseling behavior may vary. For example, when the substrate is highly anisotropic, the trajectory of the atomic catalyst may exhibit stronger directionality than what we showed here. Compared to enzymes which bind to and then modify biomaterials through thermal fluctuations, an atomic catalyst chiseling its substrate may be tuned by electron irradiation and perhaps other external stimulations, which represents a new scalable paradigm of obtaining stable nanostructures through ultimately precise modification of materials.

Methods. Our graphene samples (Graphenea) were synthesized using a standard chemical vapor deposition (CVD) process, followed by wet transfer to standard TEM grids. The suspended graphene samples were imaged with the TEAM 0.5 at the National Center of Microscopy (NCEM), a monochromated and aberration-corrected TEM operated at 80 kV. A negative third-order geometric aberration[25] of −15 μm and a positive defocus of 9 nm was used to balance the effects of the measured fifth-order aberration, minimizing the delocalization fringes which otherwise would degrade the atomic resolution at the edge (see the Supporting Information). We record movies of the dynamic processes with an exposure time of 1 s for each frame to optimize the trade off between lower noise level and higher tempo resolution. Phonon motions and partial coherence effects were taken into account in our simulation together with the measured noise level from the

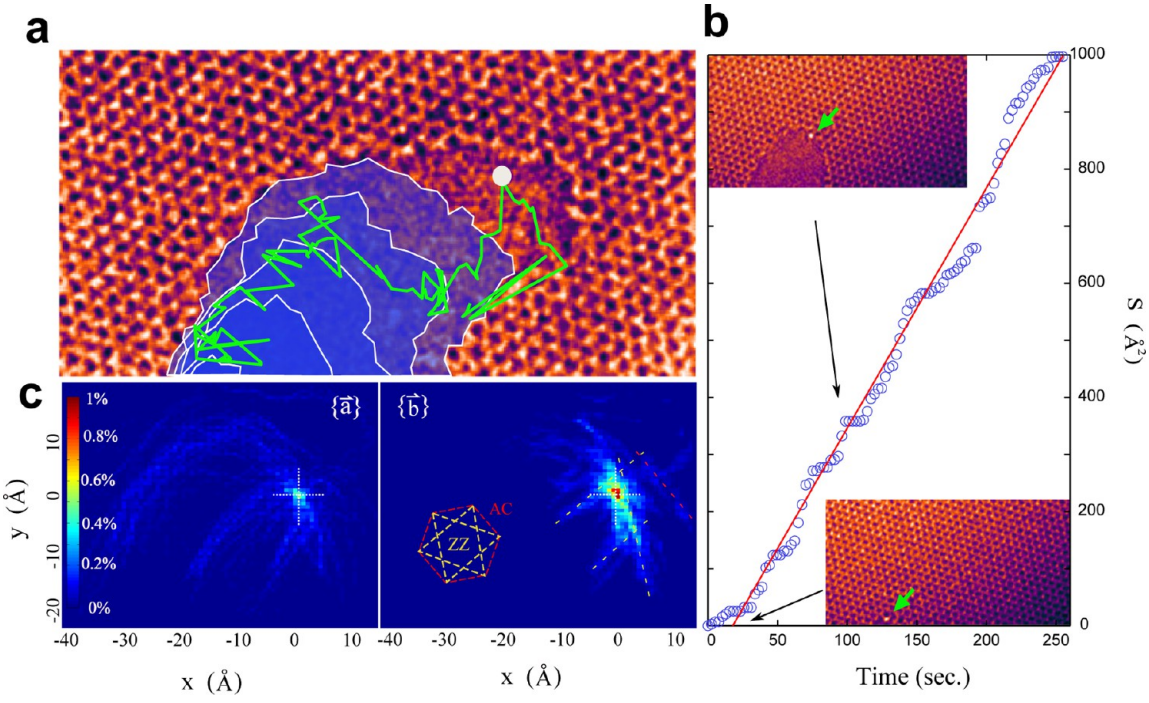

Figure 4. Dynamics of the single-atom Si chisel. (See Movie S2 in Supporting Information.) (a) The background image is a filtered snapshot from the movie showing a single Si atom catalyzing the growth of a pore in graphene. The green line is the observed trajectory of the Si atom, which consists of straight line segments connecting instantaneous positions of the Si atom in 100 snapshots. The time interval between the snapshots is 2.6 s. Five edge history lines are shown in the same image with a time interval of 20 frames. (b) The area of the hole plotted as a function of time. The linear trend indicates that the removal of C atoms is mainly due to the catalytic effects of the single Si atom. (c) Spatial distribution of two vector sets: $\{\vec{a}\}$ on the left is the "Si-edge" vector drawn from the position of the Si atom to all edge pixels; $\{\vec{b}\}$ on the right is the "Si- removed edge" vector drawn from the Si position to all pixels of graphene sites that have just been removed. The latter are determined by comparing two sequential images in the snapshot time series. Both distributions include the data from the 100 frames of images. The crystalline orientations including all the zigzag (ZZ) (yellow) and armchair (AC) (red) directions are plotted in the right panel for comparison with the anisotropic intensity of the distribution plot. The color bar represents the count of pixels in each bin normalized by the total pixel count.

dx.doi.org/10.1021/nl403327u | Nano Lett. 2014, 14, 450−455

CCD counts. The simulated HRTEM micrographs were generated with our customized MATLAB code based on the potentials and the multislice method described by Kirkland.[26] The electron wave was assumed to be quasicoherent with a convergence angle of 150 μrad and a defocus spread of 12 Å. For first-principles calculations, the structural relaxations and binding energies were carried out using the density functional theory (DFT) method with normconserving pseudopotentials as implemented in the SIESTA code.[27,28] First-principles MD simulations were carried out with the VASP code[29,30] with a time step of 1.6 ps. The cross sections of the carbon atoms were calculated with the relativistic effects and the motion of the carbon atoms taken into account.[12] The analysis of the acquired movies is conducted with our image processing code built on the Matlab Image Processing Toolbox.

■ ASSOCIATED CONTENT

Supporting Information

Supporting video files and additional discussions including the details of the fabrication, characterization, and simulation methods. This material is available free of charge via the Internet at http://pubs.acs.org.

■ AUTHOR INFORMATION

Corresponding Author

*E-mail: kaxiras@physics.harvard.edu.

Author Contributions

W.L.W, B.J., and J.C. carried out the experiments. W.L.W., E.J.G.S., and E.D.C. performed the first-principles calculations and the data analysis. A.C., A.P., and A.Z. fabricated the graphene TEM samples. C.O. and W.L.W. performed the TEM simulations. W.L.W., E.K., and R.W. wrote the manuscript. All authors read and commented on the manuscript.

Notes

The authors declare no competing financial interest.

■ ACKNOWLEDGMENTS

W.L.W. acknowledges the support from the Massachusetts Green High-Performance Computing Center (MGHPCC) and DOE grant number DE-FG02-07ER46422. This work was performed in part at NCEM, which is supported by the Office of Science, Office of Basic Energy Sciences of the U.S. Department of Energy under Contract No. DE-AC0205CH11231. Part of the calculations were performed at the Extreme Science and Engineering Discovery Environment (XSEDE), supported by NSF grant numbers TGPHY120034, TG-DMR120049, and TG-DMR120073.

■ REFERENCES

(1) Heiz, U.; Landman, U. *Nanocatalysis*; Springer: New York, 2007.

(2) Li, W. Z.; et al. Large-scale synthesis of aligned carbon nanotubes. *Science* **1996**, *274*, 1701−1703.

(3) Atthipalli, G.; et al. Nickel Catalyst-Assisted Vertical Growth of Dense Carbon Nanotube Forests on Bulk Copper. *J. Phys. Chem. C* **2011**, *115*, 3534−3538.

(4) Oh, S. H.; et al. Oscillatory Mass Transport in Vapor-Liquid-Solid Growth of Sapphire Nanowires. *Science* **2010**, *330*, 489−493.

(5) Matthiesen, J.; et al. Observation of All the Intermediate Steps of a Chemical Reaction on an Oxide Surface by Scanning Tunneling Microscopy. *ACS Nano* **2009**, *3*, 517−526.

(6) Qiao, B. T.; et al. Single-atom catalysis of CO oxidation using Pt-1/FeO_x. *Nat. Chem.* **2011**, *3*, 634−641.

(7) Lee, J.; et al. Direct visualization of reversible dynamics in a Si_6 cluster embedded in a graphene pore. *Nat. Commun.* **2013**, *4*, 1650.

(8) Geim, A. K.; Novoselov, K. S. The rise of graphene. *Nat. Mater.* **2007**, *6*, 183−191.

(9) Son, Y. W.; Cohen, M. L.; Louie, S. G. Half-metallic graphene nanoribbons. *Nature* **2006**, *444*, 347−349.

(10) Wang, W. L.; Yazyev, O. V.; Meng, S.; Kaxiras, E. Topological Frustration in Graphene Nanoflakes: Magnetic Order and Spin Logic Devices. *Phys. Rev. Lett.* **2009**, *102*, 157201.

(11) Fischbein, M. D.; Drndic, M. Sub-10 nm device fabrication in a transmission electron microscope. *Nano Lett.* **2007**, *7*, 1329−1337.

(12) Meyer, J. C.; et al. Accurate Measurement of Electron Beam Induced Displacement Cross Sections for Single-Layer Graphene. *Phys. Rev. Lett.* **2012**, *108*, 319−322.

(13) Bell, D. C.; Lemme, M. C.; Stern, L. A.; Williams, J. R.; Marcus, C. M. Precision cutting and patterning of graphene with helium ions. *Nanotechnology* **2009**, *20*, 455301.

(14) Russo, C. J.; Golovchenko, J. A. Atom-by-atom nucleation and growth of graphene nanopores. *Proc. Natl. Acad. Sci. U.S.A.* **2012**, *109*, 5953−5957.

(15) Campos, L. C.; Manfrinato, V. R.; Sanchez-Yamagishi, J. D.; Kong, J.; Jarillo-Herrero, P. Anisotropic Etching and Nanoribbon Formation in Single-Layer Graphene. *Nano Lett.* **2009**, *9*, 2600−2604.

(16) Schaffel, F.; et al. Atomic Resolution Imaging of the Edges of Catalytically Etched Suspended Few-Layer Graphene. *ACS Nano* **2011**, *5*, 1975−1983.

(17) Tapaszto, L.; Dobrik, G.; Lambin, P.; Biro, L. P. Tailoring the atomic structure of graphene nanoribbons by scanning tunnelling microscope lithography. *Nat. Nanotechnol.* **2008**, *3*, 397−401.

(18) Ramasse, Q. M.; et al. Direct Experimental Evidence of Metal-Mediated Etching of Suspended Graphene. *ACS Nano* **2012**, *6*, 4063−4071.

(19) Zan, R.; Ramasse, Q. M.; Bangert, U.; Novoselov, K. S. Graphene Reknits Its Holes. *Nano Lett.* **2012**, *12*, 3936−3940.

(20) Zan, R.; Bangert, U.; Ramasse, Q.; Novoselov, K. S. Interaction of Metals with Suspended Graphene Observed by Transmission Electron Microscopy. *J. Phys. Chem. Lett.* **2012**, *3*, 953−958.

(21) Girit, C. O.; et al. Graphene at the Edge: Stability and Dynamics. *Science* **2009**, *323*, 1705−1708.

(22) Xian, L. D.; Chou, M. Y. Diffusion of Si and C atoms on and between graphene layers. *J. Phys. D: Appl. Phys.* **2012**, *45*, 455309.

(23) Garaj, S.; et al. Graphene as a subnanometre trans-electrode membrane. *Nature* **2010**, *467*, 190−193.

(24) Boukhvalov, D. W.; Katsnelson, M. I. Destruction of graphene by metal adatoms. *Appl. Phys. Lett.* **2009**, *95*, 023109.

(25) Jia, C. L.; Lentzen, M.; Urban, K. Atomic-resolution imaging of oxygen in perovskite ceramics. *Science* **2003**, *299*, 870−873.

(26) Kirkland, E. J. *Advanced computing in electron microscopy*; Springer: New York, 2010.

(27) Soler, J. M.; et al. The SIESTA method for ab initio order-N materials simulation. *J. Phys.: Condens. Matter* **2002**, *14*, 2745−2779.

(28) Perdew, J. P.; Burke, K.; Ernzerhof, M. Generalized gradient approximation made simple. *Phys. Rev. Lett.* **1996**, *77*, 3865−3868.

(29) Kresse, G.; Furthmuller, J. Efficient iterative schemes for ab initio total-energy calculations using a plane-wave basis set. *Phys. Rev. B* **1996**, *54*, 11169−11186.

(30) Kresse, G.; Hafner, J. Ab Initio Molecular-Dynamics for Liquid-Metals. *Phys. Rev. B* **1993**, *47*, 558−561.